# Cytosol-Membrane Interface of Human Erythrocytes

**ARTICLE** *in* BIOPHYSICAL JOURNAL · APRIL 1983

Impact Factor: 3.97 · DOI: 10.1016/S0006-3495(83)84448-8 · Source: PubMed



**2 AUTHORS**, INCLUDING:

Josef Eisinger
Icahn School of Medicine at Mount Sinai
**136** PUBLICATIONS **4,168** CITATIONS

# CYTOSOL-MEMBRANE INTERFACE OF HUMAN ERYTHROCYTES

## A Resonance Energy Transfer Study

JOSEF EISINGER AND JORGE FLORES
*Bell Laboratories, Murray Hill, New Jersey 07974*

ABSTRACT The resonance energy transfer from donors embedded in the membrane of erythrocytes to the cytosol hemoglobin has been measured by comparing the donors' fluorescence decay in ghosts and in intact cells. A series of *n*-(9-anthroyloxy) stearic acids (*n*-AS) ($n = 2, 6, 9, 12$) and similar probes were used as donors, and their locations within the outer leaflet of the phospholipid bilayer were determined from their average efficiency of energy transfer, $\langle T \rangle$. The energy transfer data for several membrane probes were analyzed according to a simple semiempirical model, in which the heme acceptors are assumed to form a semiinfinite continuum beyond a plane, whose normal distance ($d$) from particular donors may be determined if the heme density in the cytosol boundary layer is known. The hemoglobin concentration in the erythrocytes was varied by suspending the cells in buffers of different ionic strengths. This made it possible to study the ionic strength dependence of the heme concentration averaged over the cell ($h_c$), as well as that in the boundary layer ($h_b$). Both level off above approximately 600 mosM, as does the ratio $h_b/h_c$. By using the maximum heme concentration that can be obtained in osmotically shrunken cells as a limiting value, $h_b$ is estimated to be 17 mM or less, under physiological conditions; and from the measured $\langle T \rangle$ for various probes, the distance $d$ was found to range from 40 Å for 2-AS to 31 Å for 12-AS and 26 Å for 9-vinyl anthracene (9-VA). It is concluded that the hydrophobic probe 9-VA is located near the center of the phospholipid bilayer and that the cytosol hemoglobin is in contact with the inner membrane surface, or nearly so. This conclusion is valid for oxy- and deoxy-hemoglobin, and is shown to be independent of several systematic errors that might arise from the simple assumptions of the model used. The steady-state fluorescence anisotropy of the probes was found to decrease as they approach the bilayer's central plane. The methodology developed here may be used to extend studies of cytosol membrane interactions in ghost systems to intact cells, and is useful in the investigation of the morphology of normal and pathological intact erythrocytes.

## INTRODUCTION

Recent studies have demonstrated that the biochemical interactions that occur at the cytosol-membrane interface of erythrocytes play an important role in the control of many membrane functions. Observations of specific binding to the erythrocyte membrane of glycolytic enzymes, cytoskeletal proteins, and hemoglobin have raised the question of the significance of these interactions for the transport and shape characteristics of the cell and of their physiological significance in general (Salhany and Gaines, 1981; Wilson, 1978).

While the cytosol-membrane interface of intact erythrocytes is, by its nature, not readily accessible to biochemical experimentation, resonance energy transfer (RET) from donors in the membrane to cytosol acceptors appears to be particularly well suited for exploring the geometry and dimensions of this system (Waggoner and Stryer, 1970): The range of RET, characterized by the Förster distance, is of the same order of magnitude as the membrane thickness (~40 Å), and since the efficiency of RET is a strong function of distance, donors within the membrane are insensitive to quenchers beyond a cytosol boundary layer whose thickness is on the order of a Förster distance.

In this study, fluorescent donor probes were embedded in the outer leaflet of the phospholipid bilayer portions of intact erythrocytes, and the efficiency of RET was used to estimate the distance from them to the hemes of the cytosol hemoglobin. We observed in this way that for the series of *n*-(9-anthroyloxy)-stearic acid probes (*n*-AS, with $n = 2, 6, 9, 12$), the average efficiency of energy transfer, $\langle T \rangle$, increased monotonically with increasing $n$ (Eisinger and Flores, 1982). This shows that the *n*-AS donors are indeed located in the outer phospholipid bilayer and that the depth of their anthroyloxy groups increases with $n$. Their distance from the nearest hemes of the cytosol hemoglobin can be estimated from $\langle T \rangle$ and from the heme concentration in the cytosol boundary layer, which may in turn be estimated from the dependence of $\langle T \rangle$ on the ionic

strength of the suspending medium, and hence the volume, of the erythrocytes. The average efficiency of RET was determined by comparing the fluorescence yields of the membrane donors in intact erythrocytes with those in ghosts, i.e., in the presence and absence of acceptors. Because these two systems have very different absorbance and scattering properties, their yields can best be compared by measuring the donors' decay kinetics, using right-angle geometry for the ghosts and front face geometry for the intact cells (Eisinger and Flores, 1979).

Similar techniques based on transverse resonance energy transfer (i.e., across the membrane) have recently been used to study the pH-dependent approach or binding of cytosol hemoglobin to fluorescent DIDS (4,4'-bis(isothiocyano)-2-2'-stillbene disulfonate) donors attached to the integral membrane protein band 3 in intact erythrocytes (Eisinger et al., 1982). The binding of hemoglobin to erythrocyte ghosts had previously been observed under conditions of low pH and low ionic strength by RET and light scattering experiments (Shaklai, et al., 1977; Salhany et al., 1977). In the present study we measure the proximity and concentration of the cytosol hemoglobin layer in intact erythrocytes under physiological conditions. In doing so a model and experimental protocol are developed that make it possible to make quantitative comparisons of the cytosol membrane interfaces of normal erythrocytes and of pathological ones, such as sickle cells. (Eisinger, Flores and Bookchin, in preparation).

## METHODS

### 1. Sample Preparation

Blood was collected in heparinized containers from healthy casual donors and was generally used within 24 h. The erythrocytes were washed three times in isotonic buffer containing 10 mM Na phosphate, pH 7.4, 0.15 M NaCl (PBS), before being labeled with *n*-AS or other fluorescent probes. The fluorescence characteristics of labeled cells remained unchanged for 48 h after labeling, which indicates that the probes did not partition appreciably to the inner bilayer or into the cytoplasm. Labeled ghosts were obtained by lysis of labeled cells.

*n*-(9-anthroyloxy) stearic acids and palmitic acids (*n*-AP), were purchased from Molecular Probes (Plano, TX) and stock solutions (~6 mg/ml) were prepared by dissolving them in ethyl alcohol. 9-vinyl anthracene (9-VA) was obtained from Aldrich Chemical Co., Inc. (Milwaukee, WI). Typically, 30 $\mu$l of stock solution was added to 5 ml of erythrocytes in PBS, hematocrit 0.2. The cells were then incubated for 45 min at room temperature and washed with PBS. To lyse labeled cells, 1 ml of packed erythrocytes was diluted with 45 ml of 5 mM Na phosphate buffer, pH 8 (5P8) at 4°C. After 10 min the ghosts were centrifuged at 10,000 rpm for 10 min and were subsequently washed three times with 5P8.

The titre of ghost suspensions was determined by measuring their optical absorbance at 280 nm in 1% sodium dodecyl sulfate (SDS). Under these conditions small phospholipid-detergent micelles are formed, and scattering is greatly reduced. As a result, the 280 nm absorbance peak of the membrane proteins could be resolved, and was found to be linear with the titre as determined by means of a Coulter counter, with (2.15 ± 0.1) × $10^9$ ghosts/ml corresponding to 1 AU (arbitrary unit) (280 nm) (see Fig. 1).

The number of probes in a ghost suspension was measured by absorption spectroscopy, using 8.2 × $10^3$ $cm^{-1}$ as the molar extinction coefficient of all *n*-AS and *n*-AP probes, and for 9-VA. The *n*-AS fluorescence spectrum and steady-state anisotropy ($\langle r \rangle$) remained constant while fluorescence quantum yield ($\phi$) decreased by only a few percent from its low probe limit for labeling ratios of up to 2 × $10^7$ probes per cell, and all experiments were performed with labeling ratios below this value (see Figs. 2 and 3). The buffers used in the experiments in which the ionic strength of the suspending medium was varied were adjusted by NaCl, and their ionic strengths (in mosM) were measured by means of a freezing point depression apparatus (Advanced Instruments Inc., Needham Heights, MA, model 3W). The hemoglobin (or heme) concentration of samples was determined by adding Reagent Hycel 116-00 (Hycel, Inc., Houston, TX) to form cyano-met-hemoglobin, and measuring the absorption spectrum, using $\epsilon$(540 nm) = 11,500 $cm^{-1}$ $M^{-1}$. Hematocrits were measured by means of a Readacrit centrifuge (Clay Adams Div., Parsippany, NJ).

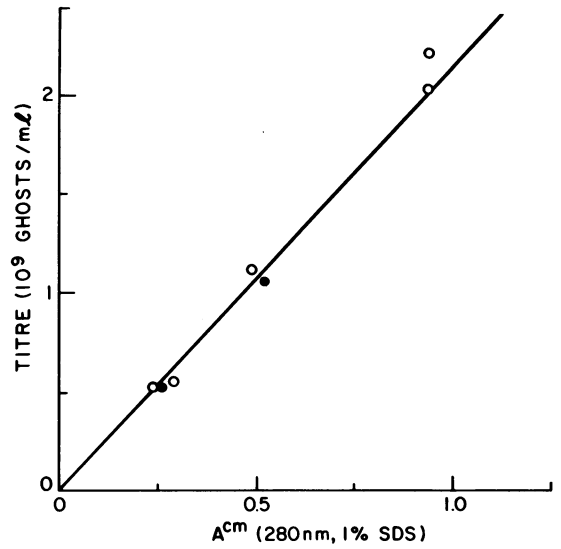


FIGURE 1 The titre of erythrocyte ghost suspensions determined by means of a Coulter counter plotted against their absorbance at 280 nm, following the addition of 1% SDS. The actual absorbance measurements were made using suitably diluted aliquots. The slope of the line shown fitted to the data corresponds to 2.15 × $10^9$ ghosts/ml per AU (280 nm).

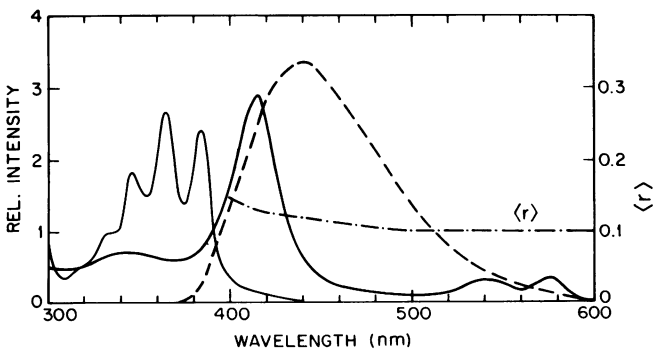


FIGURE 2 The absorption spectra of 12-AS in ghosts (with 1% SDS) and of hemoglobin are shown by the light and heavy curves, respectively. The dashed curve (---) is the 12-AS fluorescence spectrum that is seen to have a good overlap with the heme absorption spectrum. The wavelength dependence of the 12-AS emission anisotropy, $\langle r \rangle$, is also shown. The excitation wavelength was 350 nm, and the temperature 22°C.

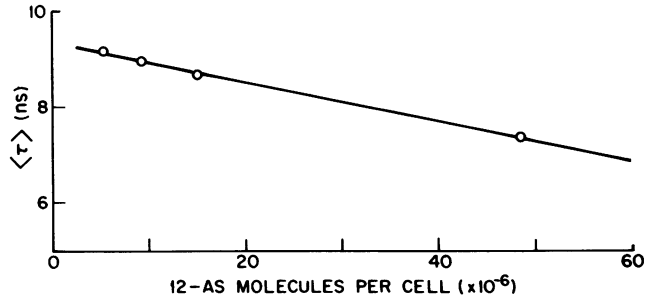


FIGURE 3 The average lifetime, $\langle \tau \rangle$, of 12-AS in the membrane of intact cells as a function of the labelling ratio. The linear decrease in $\langle \tau \rangle$ is consistent with self-transfer.

## 2. Fluorescence Instrumentation and Analysis

Corrected steady-state fluorescence emission and polarization spectra were obtained by means of a greatly modified SLM spectrofluorometer (SLM Instruments Inc., American Instrument Co., Champaign, IL) using two symmetrically placed monochromators for the vertically and horizontally polarized components ($I_V$, $I_H$) of fluorescence. Total fluorescence, $I_T = I_V + 2I_H$, and the emission anisotropy, $\langle r \rangle = (I_V - I_H)/I_T$, were corrected for differences in the wavelength-dependent efficiencies of the two emission-detector systems in the usual manner, by comparing the observed $I_V$ and $I_H$ from a fluorescent sample excited by horizontally polarized light. Excitation light was provided by a 500 W xenon arc and a double monochromator equipped with holographic gratings. Hamamatsu Corp. (Middlesex, NJ, model R928P) side-window photomultipliers, in a single-photon counting mode, were used as detectors, and the digital signals were processed by a PDP 11/34 computer (Digital Equipment Corp., Marlboro, MA), which also operated the wavelength drives of the spectrofluorometer. An *X-Y* recorder (Hewlett-Packard Co., Palo Alto CA) provided graphical display for emission, excitation, and polarization spectra. Quantum yields were calculated from the integrated $I_T$ spectra, obtained with optically thin samples and using $\phi = 0.55$ for a quinine sulfate solution in 1N $H_2SO_4$ as a standard (Eisinger et al. 1981).

Fluorescence decays were measured by means of a specially constructed high-speed filter fluorometer, using f/2 Quartz lenses for the excitation and emission optics. A high-pressure hydrogen spark lamp (EEY Scientific, La Jolla, CA) was the excitation source and was operated at ~12 kV and ~25 kHz. It provides an intense excitation pulse whose half-width, as measured with a glycogen scattering sample and an RCA C31034-02 photomultiplier (RCA Electro-Optics & Devices, Lancaster, PA), was ~2 ns. This lamp is exteremely stable, and its intensity vs. time profile decays exponentially over more than three decades of intensity and remains constant over periods of many hours. By using interference filters with excellent blocking characteristics (Melles-Griot, Irvine, CA) and minimizing internal scattering, the background photon rate of this fluorometer was reduced to less than ~1 $s^{-1}$, even with front face cells and strongly absorbant samples for which a few hundred fluorescence photons per second were detected. A time-to-amplitude converter (Ortec Inc., EG&G Inc., Oak Ridge, TN, model 437) and 128-channel pulse height analyzer (Nuclear Data, Inc., Schaumburg, IL) were used to obtain the fluorescence decay data. Data collection generally required <30 min with $10^4$–$10^5$ photons acquired in the highest intensity channels. Later experiments, which yielded most of the data presented here, made use of a Tracor Northern (Middletown, WI, model TN-1750) pulse-height analyzer. 512 channels of ~0.4 ns width each were used for each decay profile.

Experimental fluorescence decays represent the fluorophore decay functions convoluted by the excitation lamp profile, and were analyzed in two ways. They could be fitted extremely closely over three decades of intensity by using an interactive plotting program developed by W. E. Blumberg (Bell Labs, Murray Hill NJ) in which the experimental data are compared with multi-exponential impulse decay function.

$$I(t) = \sum_i \alpha_i \exp(-t/\tau_i) \tag{1}$$

convoluted by the experimental excitation lamp profile. If $E(t)$ represents the excitation profile measured by use of a scattering sample, the convoluted decay is given by

$$I_{CV}(t) = \int_0^t E(t')I(t - t')dt'. \tag{2}$$

Usually, two exponential decay times were sufficient to characterize the probes' decays and their values, $\tau_i$, were generally within a factor of 2 of

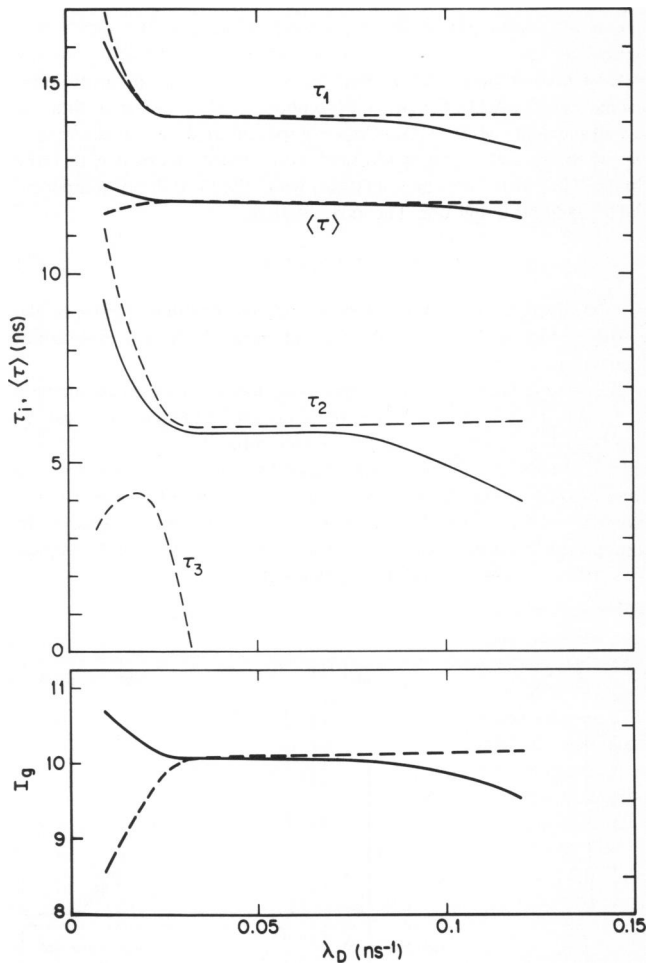


FIGURE 4 Analysis of the decay of the 12-AS in ghosts by the method of moments. The upper part shows the lifetimes ($\tau_i$) obtained in a second moment deconvolution of the experimental decay, as a function of $\lambda_D$, the exponential depression parameter in $ns^{-1}$. The solid (—) and dashed (---) curves correspond to two- and three-component exponential impulse decay functions. The correct $\tau_1$ and $\tau_2$ values are obtained from the flat portions ($\lambda_D \approx 0.05$ $ns^{-1}$). Note that the average lifetime, $\langle \tau \rangle$ is almost independent of $\lambda_D$ over the range shown. The integrated intensity ($I_g$), which is used in the determination of $\langle T \rangle$, is shown in the lower portion of the figure and near $\lambda_D \sim 0.05$ $ns^{-1}$; it is flat and independent of the number of components assumed in the analysis. The intensity contributed by the third component ($\tau_3$) is almost negligible, as indicated by the similarity of $\tau_1$ and $\tau_2$ for two- and three-component analyses.

each other. For weakly emitting and strongly absorbing samples, such as intact erythrocytes measured in the front face configuration, it was necessary to include an admixture of the exciting pulse profile to obtain a satisfactory agreement between experiment and $I_{cv}(t)$, the convoluted impulse response function. The magnitude of this scattering contribution was, as expected, inversely proportional to the fluorescence yield, and was generally <10% of the total detected fluorescence.

Alternatively, the impulse response function, $I(t)$, was determined from the experimental decay profile by the "method of moments" deconvolution procedure developed by Isenberg and his collaborators (Isenberg and Dyson, 1969; Isenberg et al., 1973). It has been shown that with the use of first and higher moments, $I(t)$ is insensitive to possible time shifts between the observed excitation and fluorescence profiles as well as to contributions of scattered light contained in the fluorescence data. Exponential depression (Small and Isenberg, 1981) was used to improve the accuracy of the deconvolution, and $\alpha_i$ and $\tau_i$ values were chosen by requiring that the $\tau_i$'s be independent of the exponential depression constant $\lambda_D$, over a range of $\lambda_D$. The adequacy of the biexponential impulse decay function was tested by "moment index displacement" (MD) (Small and Isenberg, 1977). When a first- or second-moment (MD1, MD2) three-component analysis was attempted, two of the $\alpha_i$ and $\tau_i$ values returned were almost identical with those obtained in a two-component analysis, while the third decay component had a negligible amplitude. The mean lifetime,

$$\langle \tau \rangle = \Sigma \alpha_i \tau_i^2 / \Sigma \alpha_i \tau_i, \tag{3}$$

was almost identical for two- and three-component analyses, and was, like $\alpha_i$ and $\tau_i$, independent of $\lambda_D$ for the appropriately chosen exponential depression. (cf. Fig. 4.)

The two methods used for the determination of the decay parameters $\alpha_i$, $\tau_i$ yielded virtually identical impulse response functions. This can be seen from Fig. 5, which shows the biexponential decay obtained by the method of moments following convolution by the excitation profile (---) superimposed on the experimental fluorescence profiles. The fit was excellent over at least three decades of intensity in all cases, if an appropriate scattering contribution was included for intact cell samples. No scattering allowance was necessary for ghosts.

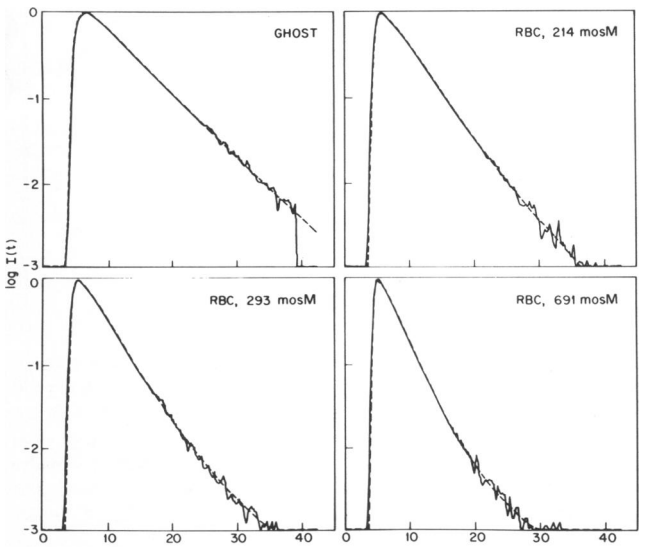


FIGURE 5 The experimental logarithmic fluorescence decay profiles of 9-VA in ghosts and intact erthrocytes at different ionic strengths. The dashed curves (---) represent the biexponential impulse decay functions obtained by the method of moments and convoluted with the excitation pulse.

The analysis outlined above suggests that a biexponential impulse function offers an adequate description of the probe's decay kinetics, and that the two decay times correspond approximately to two probe conformations or environments.[1] Due to this heterogeneity in the donor population as well as to the distribution of donor-quencher distances, the donor decay rates in the presence of RET are not expected to be homogeneous. Very short decay components are not, however, expected, since all probes are in the outer bilayer or (in the case of 9-VA) between the phospholipid leaflets; this is confirmed by the magnitude and relatively narrow range of decay times observed for intact erythrocytes.

With the $\alpha_i$ and $\tau_i$ determined as described above, the integrated fluorescence intensity is given by

$$I = \int_0^\infty I(t)\mathrm{d}t = \sum_i \alpha_i \tau_i \tag{4}$$

with $\Sigma \alpha_i = 1$.

If $I_{D,A}$ and $I_D$ are the integrated fluorescence intensities of the donors in the presence and absence of acceptors respectively, the average RET efficiency is therefore given by

$$\langle T \rangle = 1 - I_{D,A}/I_D. \tag{5}$$

It should be noted that although the RET efficiency is here defined in terms of an integrated intensity ratio, the fluorescence yields are obtained from the integrated impulse decay functions. The steady-state fluorescence yields cannot be used because the samples that are compared (i.e., cells and ghosts) have such different absorption and scattering properties that a direct intensity comparison would yield insufficient accuracy.

## 3. Model and Analysis for Transverse RET Experiments

To interpret transverse RET experiments in terms of the proximity and concentration of acceptors, we use the semi-empirical model illustrated in Fig. 6. This model simplifies the geometry and dynamics of the donors in the membrane and the cytosol heme acceptors, while preserving the functional dependence of $\langle T \rangle$ on the donor-acceptor separation and on the density of acceptors. It will be shown in the next section that the errors in the probe-heme separation introduced by the approximations of this model may be estimated by general considerations and are modest in magnitude. It is clear, however, that the absolute distances derived in this study are less precise than the measured experimental parameters or the relative distances or heme concentrations derived from the efficiencies of RET.

In the model of Fig. 6, all donors are at the same depth $a$ from the outer face of the bilayer, and are assumed to be distributed randomly in the lipid portion of the membrane. At the usual level of probes ($\leq 10^7$ per cell), the average separation between them is, therefore, 25 Å or more. The hemes are assumed to be uniformly and continuously distributed and are constrained to the semiinfinite space bounded by a plane whose normal distance from the donor $D$ is $d$ Å. The acceptor transition moments (planar in the case of hemes) are assumed to be oriented at random, and their orientations are averaged dynamically,[2] as are the donor transition

[1] Matayoshi and Kleinfeld (1981) have shown that the lifetimes of *n*-AS probes increase with emission wavelength and have proposed a two-state model to explain this phenomenon. While such a model would require a data analysis that differs somewhat from the one presented here, the observed emission heterogeneity varies very little over the width of the Soret absorption band of the heme. The simpler, one-state model discussed in Methods section 3 was therefore considered adequate.

[2] In dynamic orientational averaging transition dipoles adopt all possible orientations during the fluorescence lifetime. In static averaging the fluorophore orientations are stationary on this time scale. While this assumption is unjustifiable for hemes, it will be seen below that the errors resulting from it are small. (Dale et al., 1979).

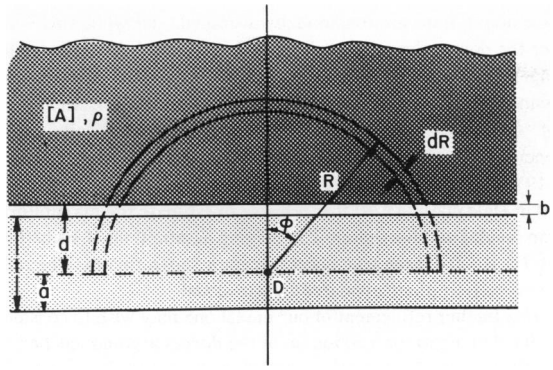


FIGURE 6 The model used for the analysis of transverse RET experiments. The acceptors ($A$), density $\rho$ per $R_0^3$, are continuously and uniformly distributed in the heavily stipled region. The donor $D$ is a distance $d$ from the acceptor boundary (cf. Methods section 3).

moments, so that the average orientation factor $\langle \kappa^2 \rangle$ is taken to be $\frac{2}{3}$ (Förster, 1948).

For a single $D$, $A$ pair the Förster distance, $R_0$, is defined as the $D$, $A$ separation at which the rate of RET equals the donor decay rate in the absence of $A$. $R_0$ may be calculated from $\langle \kappa^2 \rangle$, the donor quantum yield $\phi_D$, the index of refraction, and from the energy overlap between the donor emission and acceptor absorption spectra. At any particular $D$, $A$ separation $R$, the RET rate ($k_T$) has an inverse sixth power dependence (Förster, 1947), from the square of the dipole-dipole interaction between the transition dipoles of $D$ and $A$ that gives rise to it. If $k$ is the donor decay rate in the absence of acceptors,

$$k_T = k(R_0/R)^6. \tag{6}$$

It is convenient to express all distances in terms of $R_0$. We therefore define the dimensionless distances $x = d/R_0$ and $r = R/R_0$ and express the acceptor density $\rho$ as the number of hemes in a volume of magnitude $R_0^3$ (Wolber and Hudson, 1979). The area of a spherical shell with radius $r$, centered on $D$, which lies within the half space of acceptors, i.e., beyond a plane whose normal distance from $D$ is $x$, is therefore

$$\int_0^{\cos^{-1}(x/R)} 2\pi r \sin\phi r \, d\phi = 2\pi r^2 \left(1 - \frac{x}{r}\right), \tag{7}$$

where the angle $\phi$ is as indicated in Fig. 6. A shell of thickness $dr$ therefore contains $dN$ acceptors, where

$$dN = 2\pi\rho\left(1 - \frac{x}{r}\right) r^2 dr. \tag{8}$$

Under dynamic averaging conditions the transfer rate from $D$ to each of these acceptors is according to Eq. 6 simply $kr^{-6}$, and since all acceptors within the shell are equidistant from $D$, the transfer rate from $D$ to the acceptors within the shell is

$$k_T(r) = 2\pi\rho k\left(1 - \frac{x}{r}\right) r^{-4} dr. \tag{9}$$

Integrating over all shells with radii between $x$ and infinity, the transfer rate from $D$ to all acceptors in the half-space is therefore

$$k_T = 2\pi\rho k \int_x^\infty (r^{-4} - xr^{-5}) dr \tag{10}$$

so that

$$k_T/k = \pi\rho/6x^3. \tag{11}$$

The efficiency of transfer from a mono-exponentially decaying donor is

$$T = k_T/(k + k_T). \tag{12}$$

By combining Eqs. 10 and 11 we may therefore obtain the parameter $\rho/x^3$, which is a measure of the quenching capacity of the acceptor distribution, in terms of the transfer efficiency given in Eq. 5.

$$-\frac{\rho}{x^3} = \frac{6}{\pi}\frac{T}{1-T}. \tag{13}$$

If $I_c$ and $I_g$ represent the fluorescence yields of the donor in intact cells and ghosts, respectively, $T$ may be expressed in terms of these parameters according to Eq. 5 and $\rho/x^3$, averaged over all donors and cytosol heme distributions, is

$$\left\langle \frac{\rho}{x^3} \right\rangle = \frac{6}{\pi}\left[\frac{I_g}{I_c} - 1\right]. \tag{14}$$

The dependence of $T$ on the dimensionless acceptor concentration $\rho$ and on $x$, the separation between plane of donors and the boundary plane of the acceptor sea, is illustrated in Fig. 7.

In real erythrocytes, the heme acceptors are of course not continuously distributed but discrete and grouped in a tetramer. In oxy-hemoglobin the heme-heme distances are ~25–40 Å (Muirhead et al., 1967), compared with a heme separation of ~44 Å when averaged over the volume of an erythrocyte. In spite of the high concentration of the cytosol hemoglobin (34 g/dl under physiological conditions) the scattering of x rays by hemoglobin in intact erythrocytes shows that hemoglobin remains in solution in isotonic and osmotically shrunken cells, the highest attainable concentrations being ~58 g/dl (Bateman et al., 1953; Perutz, 1948).

It must also be borne in mind that the boundary of the cytosol hemoglobin may not be sharp as assumed in our model. The parameter $\rho/x^3$ (cf. Eqs. 14 and 15) is therefore averaged over the sigmoidal density distribution so that $\rho$ represents the average heme concentration in a boundary layer whose width is at most on the order of $R_0$, i.e., ~40 Å for

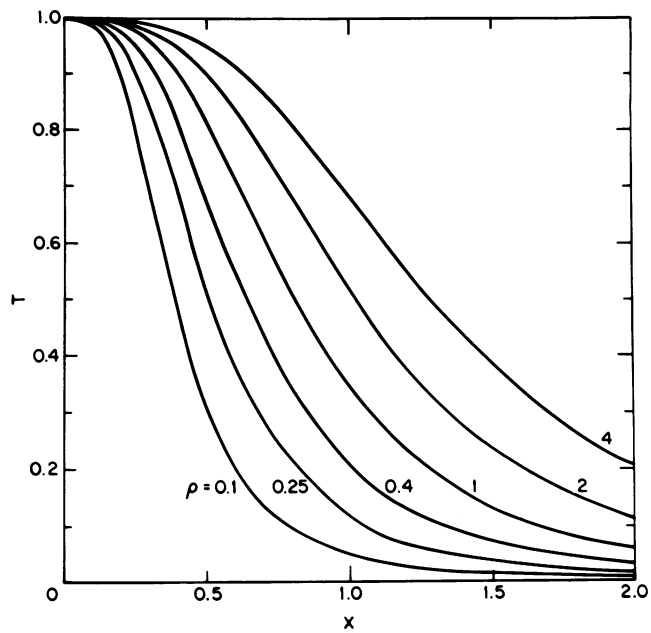


FIGURE 7 The efficiency of resonance energy transfer from a donor, $D$, to a semiinfinite continuum of acceptors. The normal distance from $D$ to the acceptor boundary is $x$ in units of $R_o$. The density $\rho$ is given in units of acceptors per volume $R_0^3$ (cf. Methods section 3).

the donors used in this study. Hemes beyond this distance have a negligible quenching effect. Layers of adsorbed proteins or other molecules may, moreover, cause the effective membrane thickness to vary from location to location. This will not be considered here except for the case in which a small fraction of the inner membrane surface might be occulted from approach by hemoglobin (by spectrin, for example).

$\rho$ is of course related to $h_b$, the heme concentration in the boundary layer. If $N_A$ is Avogadro's number, $R_0$ is in Å, and $h_b$ is in millimolarity

$$\rho = 10^{-30} N_A h_b R_0^3. \quad (15)$$

Using Eq. 15 in Eq. 13 we may therefore express $d$, the absolute distance between the donor and the heme boundary layer, in terms of $h_b$ (millimolarity), $R_0$ (angstroms) and the observed transfer efficiency.

$$d(\text{Å}) = 0.0068[h_b(T^{-1} - 1)]^{1/3} R_0^2. \quad (16)$$

## 4. Error Analysis

Having presented a model for the analysis of energy transfer experiments, the potential systematic errors arising from the assumptions of the model will be considered.

(*a*) The assumption that the acceptors are distributed uniformly has the consequence that all donors are exposed to identical acceptor distributions. It is demonstrated in the Appendix that "lumpiness" in the acceptor distribution results in a slightly lower RET efficiency than is predicted by Eq. 13, but the effect on $T$ is unlikely to exceed a few percent and leads to slightly smaller values of $d$. The lack of sensitivity to lumpiness in the acceptor distribution is the result of the high concentration of hemoglobin within the erythrocyte (packing fraction ~ 0.3), and of the fact that the average intra- and intermolecular heme-heme distances are not very different, as we discussed in Methods section 3.

(*b*) The assumption that both donors and acceptors have random orientations is at least approximately true, since the steady-state anisotropy of the *n*-AS and 9-VA probes are small ($\langle r \rangle$ ~0.1), and the heme transition moments are planar and oriented at random. Because the transition moment of the anthroyloxy moiety of *n*-AS and *n*-AP probes in lecithin vesicles was determined to be parallel to the short axis of the molecule (Badley et al., 1973), the donor transition moments can be expected to lie preferentially in the membrane plane. The isotropic model presented above may therefore be refined by replacing the isotropic orientational donor distribution by one that is characterized by a dynamically averaged axial depolarization factor (Dale, et al., 1979)

$$\langle d_D^x \rangle = (r_\infty / 0.4)^{1/2}. \quad (17)$$

$r_\infty$ is the limiting value of the time-dependent emission anisotropy and is in the limit of rapid orientational diffusion about the same as $\langle r \rangle$ (Kawato et al., 1977; Dale et al., 1977). R. E. Dale (private communication, 1982) has recently shown that, within the acceptor continuum model considered here, the transfer rate from donors whose transition moments lie preferentially in the membrane plane, is given by

$$k_T^* = k_T [1 - (1/4)\langle d_D^x \rangle] \quad (18)$$

where $k_T$ is as given by Eq. 10. The Förster distance for this donor-acceptor ensemble is readily seen to be

$$R_0^* = R_0[1 - (1/4)\langle d_D^x \rangle]^{1/6} \quad (19)$$

where $R_0$ is the value calculated with $\langle \kappa^2 \rangle = 2/3$, and Eq. 16 becomes

$$d^* = 0.0068[h_b(T^{-1} - 1)]^{1/3}[1 - (1/4)\langle d_D^x \rangle]^{2/3} R_0^2. \quad (20)$$

For the *n*-AS and *n*-AP probes, $\langle d_D^x \rangle$ is estimated to be <0.5 and leads to $d^*$ values that are ~10% smaller than the $d$ values calculated for the isotropic model, which are given in Table II. The 9-VA probe emission is almost isotropic ($\langle d_D^x \rangle \approx 0$) and $d^*$ is the same as $d$.

(*c*) The model described above further assumes that the donor and acceptor orientations are dynamically averaged, and while this is nearly true for the donor, the rotational relaxation times of the acceptor hemes are longer than the donor lifetimes. The magnitude of the error caused by this assumption of dynamic averaging may be estimated from a comparison of $\langle T \rangle_d$ and $\langle T \rangle_s$, the dynamically and statically averaged efficiencies for isotropic distributions of $D$ and $A$. It has been shown (Dale et al., 1979), that $\langle T \rangle_d$ is always somewhat larger than $\langle T \rangle_s$, and from Fig. 10 in Dale et al. (1979) it is possible to estimate the maximum error that can result from the dynamic averaging assumption. If, as is the case here, $\langle T \rangle$ is <0.45, the true donor-acceptor separation may be reduced by up to 12% from that calculated by our model.

(*d*) In a further refinement of our model one may wish to consider the possibility that a certain fraction, $u$, of the donors are unquenched in the intact cell, possibly because the cytoskeleton prevents hemoglobin from approaching a portion of the lipid bilayer. If $\langle T \rangle$ is the observed transfer efficiency, the quenchable donor fraction, $1 - u$, would then be quenched with a greater efficiency, $\langle T \rangle/(1 - u)$. The normal distance between donor and the quencher boundary plane would, according to Eq. 16, be reduced to

$$d_u = d\left[\frac{1 - u - \langle T \rangle}{1 - \langle T \rangle}\right]^{1/3}. \quad (21)$$

Using a typical value of $\langle T \rangle = 0.25$ and assuming an unquenched donor fraction of 0.2, the values of $d$ would therefore be reduced by 9% (see Discussion and Summary).

The four systematic errors, *a–d*, discussed in this section all cause $d$ to be reduced from the value predicted by our model. Eq. 16 therefore yields a maximum value of $d$. Errors *a–c* can reduce $d$ by up to 25%, with an additional reduction due to an unquenched donor fraction being given in Eq. 21.

In addition to these systematic errors, $d$ is subject to a random error caused by the experimental uncertainty with which $\langle T \rangle$ is determined. Differentiation of Eq. 16 leads to the following expression for the fractional error in $d$

$$\frac{\Delta d}{d} = -\frac{1}{3(1 - \langle T \rangle)} \frac{\Delta \langle T \rangle}{\langle T \rangle}. \quad (22)$$

The fractional error in $\langle T \rangle$ is maximally 0.1. With $\langle T \rangle \sim 0.3$ the random error in $d$ is therefore ~5%.

Although in the above discussion the heme concentration is considered known with the distance $d$ to be determined, it must be remembered that $\langle \rho / x^3 \rangle$ is the derived parameter, and for certain applications the distance $x$ is considered known or invariant, with the concentration $\rho$ to be determined. A similar error analysis would apply.

# RESULTS

## 1. Probe Location

Before using the methodology for investigating the cytosol-membrane interface that is outlined in Methods section 3, the location of the donors within the membrane had to be established. To that end we inserted a series of *n*-AS probes in the membrane of intact erythrocytes and measured their decay characteristics immediately after labeling (~30 min) and again following lysis by osmotic shock and removal of the hemoglobin. The efficiency of energy transfer to the cytosol hemes was then calculated according to Eq. 5.

Fig. 8 shows the experimental decay function of the 2-AS and 12-AS in intact cells and ghosts, along with the intensity profiles of the excitation light pulses measured at

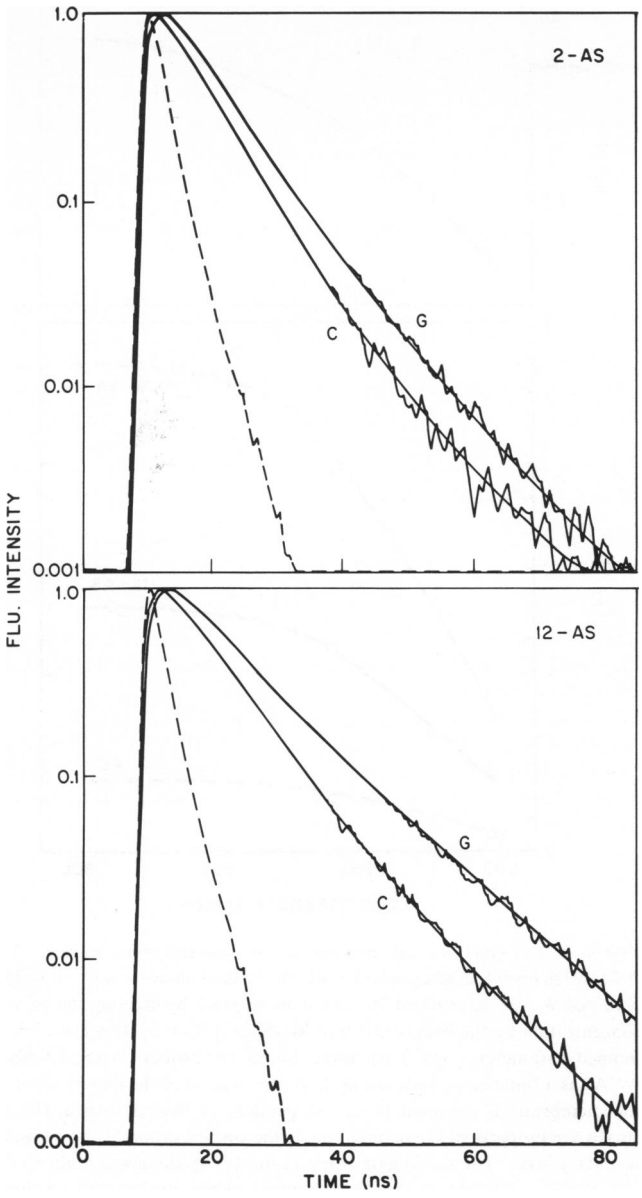


FIGURE 8 The logarithmic fluorescence intensity profiles of 2-AS and 12-AS in ghosts (*G*) and intact cells (*C*) following excitation by a narrow lamp pulse (----). The convoluted impulse decay functions determined by the method of moments, is shown superimposed on the experimental (noisy) curves. (Flu. Intensity = fluorescence intensity.)

the emission wavelength (450 nm). Even the raw data show clearly that the cytosol hemoglobin quenches the 12-AS donors more strongly than the 2-AS probes, and since the heme concentration responsible for this quenching is presumably the same in these experiments, it is concluded that the 12-AS probes are indeed located deeper in the outer leaflet of the membrane. The results of such experiments for *n*-AS probes with $n = 2, 6, 9$, and 12 are summarized in Table I. The table also includes data for 9-VA and for 2-AP and 16-AP. Among these donors only 9-VA lacks the carboxyl groups that are responsible for anchoring them in the vicinity of the head groups of the outer leaflet of the phospholipid bilayer. The most efficient RET is seen to occur from 9-VA, and a comparison of the distances *d* for the 9-VA and *n*-AS probes, respectively, suggests that 9-VA is located preferentially near the center plane of the bilayer. The somewhat anomalous behavior of 2-AP is discussed in Discussion and Summary.

The decays of 12-AS and 9-VA were also measured in paraffin oil (Exxon Primol No. 355, Exxon Co., Houston, TX) and were found to be mono-exponential to better than 99%. Their lifetimes at 22°C were 10.5 and 9.6 ns, respectively. This suggests that the biexponential decay observed in ghosts is due to a distribution of probe sites and/or conformations in that nonisotropic environment.

Table I also shows the steady-state anisotropy $\langle r \rangle$ of the various donors in ghosts. The decrease in $\langle r \rangle$ with increasing *n* suggests at first sight that the fluidity of the lipid portions of the membrane is greatest in the vicinity of the mid-plane. Qualitatively similar results have been reported in dipalmitoylphosphatidylcholine vesicles, for which the fluidity gradient across the bilayer was considerably smaller (Thulborn and Sawyer, 1978; Tilley et al., 1979). Similar results have also been reported by Matayoshi and Kleinfeld (1981), who made the interesting observation that even in paraffin oil the steady-state polarization of *n*-AS probes is a function of *n*, the emission anisotropy at 440 nm for 2-AS being almost 50% greater than that of 12-AS. This shows that the rotational mobility of the anthroyloxy group is affected not only by its environment but by the fluorophore's point of attachment to the fatty acid. It is clear from such considerations that measurements of the polarization decay characteristics are needed for a better understanding of the fluidity gradient across the membrane (Kawato et al., 1977, Dale et al., 1977), and such experiments are currently under way in our laboratory.

TABLE I
FLUORESCENCE AND RET PARAMETERS OF MEMBRANE PROBES WITH THEIR DISTANCES FROM CYTOSOL HEMOGLOBIN

| Probe | $\phi$* | ⟨r⟩‡ | $R_0$§ | $I_c$ | $I_g$ | ⟨*T*⟩‖ | $d_{min}$¶ | $d_{max}$¶ | *a*¶ |
|---|---|---|---|---|---|---|---|---|---|
| | | | (Å) | (*ns*) | (*ns*) | | (Å) | (Å) | (Å) |
| 2-AS | 0.33 | 0.19 | 33.4 | 5.91 | 6.51 | 0.09 | 29 | 40 | 10 |
| 6-AS | 0.40 | 0.18 | 34.6 | 6.62 | 8.05 | 0.18 | 24 | 36 | 14 |
| 9-AS | 0.44 | 0.17 | 35.4 | 6.85 | 8.71 | 0.21 | 23 | 32 | 18 |
| 12-AS | 0.47 | 0.13 | 36.0 | 7.15 | 9.71 | 0.26 | 22 | 31 | 19 |
| 2-AP | 0.34 | 0.11 | 32.9 | 5.36 | 6.56 | 0.18 | 22 | 30 | 20 |
| 16-AP | 0.44 | 0.05 | 34.5 | 7.04 | 9.29 | 0.24 | 21 | 29 | 21 |
| 9-VA | 0.52 | 0.03 | 37.9 | 6.41 | 11.24 | 0.43 | 19 | 26 | 24 |

*Quantum yield in white ghosts at 22°C.
‡The steady state anisotropy at $\lambda = 440$ nm.
§The Förster distances were calculated assuming complete dynamic orientational averaging, i.e., $\langle k^2 \rangle = 2/3$. See Methods section 4 for a discussion of errors arising from this assumption.
‖$\langle T \rangle = 1 - I_c/I_g$, cf. Eq. 5 $I_c$ and $I_g$ were determined from the probes' decay functions in cells in PBS and ghosts prepared from the same cells, in 5P8 buffer, both at 22°C.
¶Assumptions for calculating $d_{min}$, $d_{max}$ and *a* are given in results.

If the *n*-AS probes had a tendency to flip over and to translocate into the inner leaflet of the membrane of intact erythrocytes, it would lead to a considerably faster fluorescence decay, since RET to the cytoplasmic hemoglobin would be greatly enhanced. We measured the fluorescence decay of 2-AS labeled cells as a function of time after labeling, and could observe no change over a period of 24 h at 22°C or 1 h at 37°C. This result is consistent with the slow translocation of stearic acid from the outer to the inner leaflet (~35 h at 37°C) reported by Mohandas et al. (1980). It is interesting that the n-AS probes' translocation is as slow or slower.

## 2. The Cytosol-Membrane Interface

To derive probe-hemoglobin separations from the RET efficiencies listed in Table I, an estimate of the heme concentration in the cytosol boundary layer is needed and was obtained indirectly through a consideration of the ionic strength dependence of $\langle T \rangle$.

Raising the ionic strength of the buffer shrinks the volume of the erythrocytes and therefore raises the average hemoglobin concentration within the cells. As can be seen from the data of Fig. 9, this results in an increase in RET efficiency and a concomitant decrease in the lifetime of a membrane probe. The quenching parameter $\langle \rho/x^3 \rangle$ obtained from these data is shown as a function of ionic strength in Fig. 10, along with $h_c$, the average heme concentration within the erythrocytes, as determined from the hematocrit and total hemoglobin of the samples. According to the curves of Fig. 10, $\langle \rho/x^3 \rangle$ for the three probes 2-AS, 12-AS, and 9-VA are in the approximate ratio 0.3:1:2 over a wide range of ionic strengths. This is reasonably consistent with the implicit assumption of our model that these probes are quenched by the same hemoglobin boundary layer, but that their normal distances from it, which are inversely proportional to the cube root of

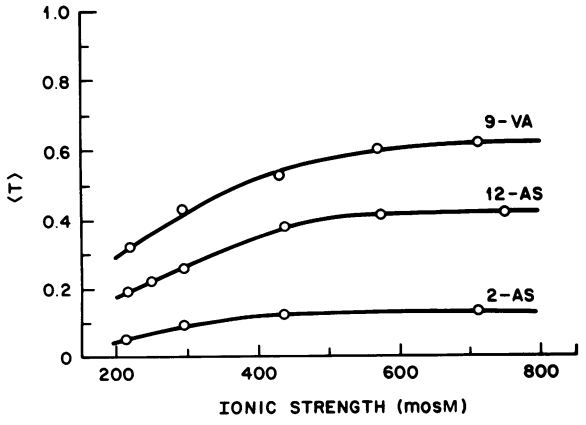


FIGURE 9 The average transfer efficiency, $\langle T \rangle$, of 2-AS, 12-AS, and 9-VA donors in intact erythrocytes and in ghosts. The cells were swollen and shrunk by being suspended in hypotonic and hypertonic buffers, respectively. Fluorescence yields were obtained as described in Methods section 2 and $\langle T \rangle = 1 - (I_c/I_g)$ (cf. Eq. 5).

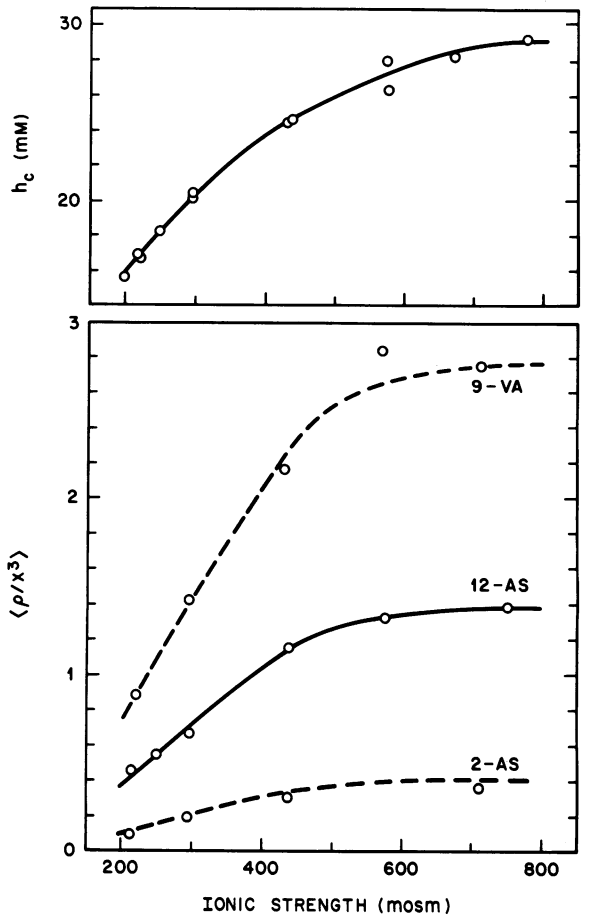


FIGURE 10 (*Top*) $h_c$, the average heme concentration in the 12-AS-labeled erythrocyte samples for which the data shown in Fig. 10 were obtained. $h_c$ was determined for each ionic strength by dividing the heme concentration by the hematocrit (see Methods section 1). (*Bottom*) The lumped parameter $\langle \rho/x^3 \rangle$ for three membrane probes (2-AS, 12-AS, 9-VA) as a function of ionic strength. If the location of the donors within the membrane is assumed to be independent of ionic strength, these curves are proportional to $\rho$, or $h_b$, the heme concentration of the cytosol boundary layer. The solid curve fitted to the 12-AS data was multiplied by 2.0 and 0.3 to obtain the dashed curves, which are seen to provide reasonable fits for the 9-VA and 2-AS data, respectively.

the above ratio (1.5:1:0.8), are in approximate agreement with the *d* values given in Table I (40:31:26 Å). $\langle \rho/x^3 \rangle$, which for a particular membrane probe is proportional to $h_b$, the heme concentration in the hemoglobin boundary layer, is seen to increase with ionic strength and level off at ~600 mosM. The data of Fig. 10 also show that the relative locations of the probes remain about the same while the cells are shrunken and dilated. The average heme molarity in the cell, $h_c$, is also seen to rise towards a limiting value and reaches ~30 mM at 800 mosM (cf. Fig. 10).

To estimate $h_b$ under physiological conditions $h_b/h_c$ was calculated for 12-AS labeled cells at different ionic strengths under two assumptions: (*a*) $h_b$ approaches $h_c$ (~30 mM) at high ionic strength and (*b*) $h_b$ approaches 34 mM, the highest heme molarity that has been observed in osmotically shrunken cells (Bateman et al., 1953). For

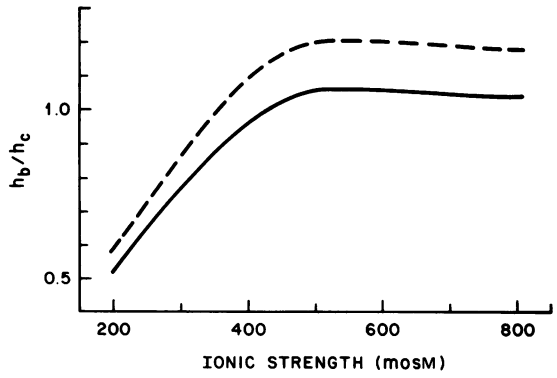


FIGURE 11 The ratio of heme concentrations in the boundary layer ($h_b$) and averaged over the cytoplasm ($h_c$), as a function of ionic strength. The solid and dashed curves correspond to the assumptions that at high ionic strength $h_b$ approaches $h_c$ (~30 mM) and 34 mM, the maximum heme concentration obtainable by osmotic shrinkage of the erythrocyte (cf. Results section 2).

these two limits, the data of Fig. 10 lead to values for $h_b$ of 15 and 17 mM, respectively, under physiological conditions (295 mosM), the latter representing a maximum estimate. Fig. 11 indicates that as the erythrocyte shrinks, the boundary layer's hemoglobin concentration increases relative to the mean cell hemoglobin concentration (MCHC), and levels off at ionic strengths >500 mosM.

We may use $h_b$ to obtain estimates for absolute values for the distance $d$. It can be seen from Eq. 16 that $h_b$ enters as a cube root in the determination of $d$, so that the fractional error in $d$ is only a third as large as the errors in $h_b$. It should be added that if the limiting value of $h_b$ at high ionic strength is substantially less than is assumed in the argument above, $d$ would be reduced accordingly.

Table I lists minimum and maximum values of $d$. $d_{max}$ was calculated by use of Eq. 16 with $h_b$ = 15 mM, while $d_{min}$ was obtained with $h_b$ = 17 mM with the systematic errors *a–c* of Methods section 3 allowed to attain their maximal values (~25% of the total). The unquenched fraction of donors, $u$, is assumed to be zero for $d_{min}$ and $d_{max}$.

The phospholipid bilayer thickness has been measured to be 40–45 Å by x-ray diffraction methods (Wilkins et al., 1971; Stamatoff et al., 1979). If we assume that the heme is 5–10 Å from the surface of hemoglobin, we conclude that $d$ for the deepest lying probes (12-AS, 9-VA) cannot be less than 30 Å. With the aid of Eq. 21 and the $\langle T \rangle \sim 0.4$ we may therefore estimate that the fraction of unquenched donors, $u$, cannot be greater than 20%. Experimental uncertainties, on the order of ±5% in the determination of $\langle T \rangle$, were not included in the computation of $d_{max}$ and $d_{min}$.

The fact that the $d$'s for the various *n*–AS probes that are listed in Table I span a range that is indeed somewhat less than the half-width of a bilayer (~20 Å) suggests that our estimate of 15 mM for $h_b$ at 295 mosM cannot be far from its true value.

It was reported recently that fluorescent probes either in the lipid portions of the membrane or attached to the trans-membrane band 3 protein of intact erythrocytes are quenched more strongly at acidic than at neutral pH (Eisinger et al., 1982). This is presumably the result of a closer approach and/or a higher concentration of the cytosol boundary layer as certain portions of hemoglobin become positively charged. Table II presents results of a series of experiments in which 12-AS labeled erythrocytes were exposed to varying pH and ionic strength, and the lumped parameter $\langle \rho/x^3 \rangle$ was evaluated from the fluorescence decay of 12-AS in the intact cells and ghosts. The efficiency of RET is seen to increase as the pH is decreased to 6.1, and the most efficient transfer occurs in a hypertonic buffer at low pH. If it is assumed that geometry of the membrane and the location of the probe are unaffected ($x$ constant), the heme molarity of the boundary may be estimated from $\langle \rho/x^3 \rangle$ and is also given in Table II. It can be seen that within the experimental uncertainties, $h_b$ calculated in this way exceeds the molarity, which can be obtained by osmotic shrinkage of erythrocytes (Bateman et al., 1953) and even crystalline hemoglobin (47 mM, Muirhead et al., 1967). This suggests that at low pH the simple geometrical model that was used to obtain $h_b$ is no longer applicable, possibly because the positively charged hemoglobin (+8 at pH 6) disturbs the bilayer structure and/or probe location by, say, partial invagination.

To discover if the rate of RET depends on the oxygenation state of the hemoglobin, the quenching of *n*-AS probes was studied for deoxygenated cells using a specially constructed anaerobic front face cell. The Förster distances calculated for the same donors, but deoxy-heme acceptors, were determined as for oxy-hemoglobin and were found to be slightly smaller, due to the well-known small blue shift in the Soret absorption band. Deoxygenation produced a negligibly small change in the average donor lifetime

TABLE II
IONIC STRENGTH AND pH DEPENDENCE OF RET IN ERYTHROCYTES LABELED WITH 12-AS

| Sample | pH | IS | $I$ | $\langle T \rangle$ | $\langle \rho/x^3 \rangle$ | $h_b$‡ |
|---|---|---|---|---|---|---|
| | | (*mosM*) | (*ns*) | | | (*mM*) |
| ghost | 7.4 | 15 | 9.65 | — | — | — |
| ghost + Hb§ | 6.25 | 15 | 3.40 | 0.65 | — | — |
| RBC | 7.4 | 293 | 7.22 | 0.25 | 0.64 | 15 |
| RBC | 6.1 | 293 | 4.49 | 0.53 | 2.19 | (51) |
| RBC | 7.4 | 635 | 5.50 | 0.43 | 1.44 | 34 |
| RBC | 6.1 | 700 | 3.75 | 0.61 | 3.00 | (70) |

*With $I_g$ = 9.65 ns.
‡The heme molarity of the boundary layer ($h_b$) was taken to be 15 mM for erythrocytes at pH 7.2, IS = 293 mosM (see Methods section 2). $h_b$ values for erythrocytes under othe conditions were obtained by assuming proportionality to $\langle \rho/x^3 \rangle$.
§End point of Hb titration of ghosts. Ghost titre was 0.55 × $10^8$ $ml^{-1}$ and heme molarity of added hemoglobin was 20 μM.

observed in intact cells, and it was concluded that the $d$ values for oxy- and deoxy cells were the same within 1–2 Å. More detailed results on the effect of deoxygenation, particularly in sickle cells will be reported elsewhere (Eisinger, Flores, and Bookchin, in preparation).

## DISCUSSION AND SUMMARY

Good evidence that the model used here is appropriate is obtained from a comparison of the experimental fluorescence decay of a membrane probe in an intact cell with one simulated by augmenting the observed decay rate of the same probe in the ghost with the RET rate derived in Eq. 11. Such comparisons for four different probes are shown in Fig. 12, and it can be seen that the agreement between the predicted and observed decay is excellent over some two decades of fluorescence intensity. This is an indication that the distribution of transfer rates responsible for the measured average transfer efficiency is consistent with that expected from the simple geometrical model of Methods section 3.

It appears from the data of Table I that the dimensions of the phospholipid bilayer are more readily reconciled with $d_{max}$ than with the $d_{min}$ values. The effective depth of the various probes from the outer membrane surface, $a$, were therefore calculated from the expression $a = t + b - d_{max}$ with $t + b = 50$ Å and are listed in Table I (cf. results section 2).

The probes' distances from the cytosol hemoglobin increase in the order 9-VA < 12-AS < 9-AS < 6-AS < 2-AS. This order can be compared with the order of these

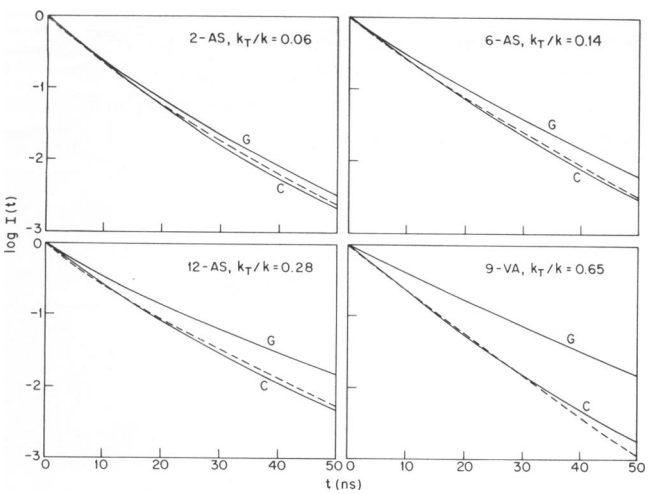


FIGURE 12 The impulse decay functions of four membrane probes (2-AS, 6-AS, 12-AS, and 9-VA) in ghosts ($G$) and intact erythrocytes ($C$). The decay parameters were those obtained in a two-component analysis by the "method of moments" and gave excellent agreement with the experiment decay profiles following convolution (cf. Eq. 2). The dashed curves (---) are the decay functions predicted from the decay functions for ghosts, if the lifetime of each component is shortened from $\tau_i$ to $(\tau_i^{-1} + k_T)^{-1}$, where $k_T = \tau_i^{-1}[\langle T \rangle^{-1} - 1]^{-1}$ (cf. Eq. 11) and $\langle T \rangle$ is the value obtained from the integrated intensities of the probe's decay in cells and ghosts (cf. Eq. 5).

and very similar probes in dimiristoylphosphatidylcholine lipisomes, as determined from the rate at which they are quenched by quenching agents either bound to the bilayer's outside surface or located near the bilayer's center. In such experiments Thulborn and Sawyer (1978) obtained the same order as that given above, but found, as we did, that 2-AP appears to be located deeper in the membrane than 2-AS, a probe that differs from it only in the length of the fatty acid chain. This anomalous behavior of 2-AP is also suggested by the probe's intrinsic quenching efficiency in solution, which is twice as great as that of $n$-AS probes (Haigh et al., 1979) and by the complexity of its infrared spectrum, which may be due to interactions between the ester and carboxylic groups (Thulborn and Sawyer, 1978). The observation that palmitic acid translocates from the outer to the inner bilayer leaflet seven times faster than stearic acid (Mohandas et al., 1980) may also help to explain the anomalous 2-AP results. Be that at is may, our experience confirms that the intramembrane location of 2-AP is poorly understood and the probe is unsuitable for experiments of the kind reported here.

The remarkable durability and flexibility of circulating erythrocyte is largely the result of the membrane skeleton, which is complexed to certain proteins at the membrane's endosurface (Lux, 1979, Branton et al., 1981). Because the cytoskeleton comprises some 60% of the membrane protein mass, its potential for interfering with the approach of hemoglobin molecules to the phospholipid area of the membrane is discussed here.

The major component (60–75% by weight) of the membrane skeleton is spectrin, whose large (~1,000 Å) slender (~50 Å) dimer (MW ~$5 \times 10^5$) is capable of forming head-to-head tetramers, but few greater aggregates (Shotton et al., 1979; Gratzer and Beavin, 1979). It is thought that the ends of these tetramers are cross-linked to actin and other proteins and that the resulting network is attached to the membrane proper by means of the spectrin-ankyrin-band 3 complexes, with only 20% of the band 3 proteins providing such points of attachment (Branton et al., 1981) Although many details of this structural model remain to be elucidated, this submembranous support system of the erythrocyte appears to be borne out by electronmicrographic evidence obtained with both isolated cytoskeletons obtained from Triton X-100 treated membranes (Sheetz and Sawyer, 1978) and with intact membranes that were rapidly frozen in liquid helium, freeze etched, and rotary shadowed (Shohet, 1981). The latter picture reveals a heavily cross-linked net formed by beaded strands (~150 Å diam.) with a mesh size of a few hundred Å. Moreover, such micrographs portray the cytoskeleton collapsed almost into a plane, while in the intact cell the spectrin network may well extend hundreds of angstroms into cytoplasm.

This model of a cytoskeletal scaffolding of considerable depth differs from the almost planar spectrin network often portrayed in models of the cytoskeleton (e.g., Lux, 1979),

but is consistent with the following consideration: The erythrocyte contains ~1.0 × $10^5$ spectrin tetramers (Fairbanks et al., 1971; Branton et al., 1981) each ~2,000 Å long. If they were assembled into a two-dimensional square meshed net with each mesh formed by four spectrin tetramers, the net would cover an area of 2,000 $\mu m^2$, which is more than 10 times the area of the erythrocyte membrane.

Because the skeleton does not appear to form an effective barrier to hemoglobin molecules (~60 Å diam.), the fraction of the phospholipid area blocked by the cytoskeleton, was taken to be zero in the analysis of our data (c.f. Methods section 4). It is of interest to consider the consequence of assuming the opposite extreme, i.e., that the protein constituting the cytoskeleton (~3 × $10^{-13}$ g/cell) forms a layer of uniform thickness along the inner membrane face. Because the membrane's surface area is 140 $\mu m^2$, the protein layer's thickness would be ~20 Å.

For the transfer efficiencies observed in these experiments and donor-heme distances of 50 Å or more, $h_b$, the heme concentration of the boundary layer, would be ~8 times greater (cf., Eq. 13). Because this is much greater than the heme concentration of crystalline hemoglobin (47 mM) it is again concluded that the phospholipid portions of the membrane is relatively accessible to cytosol hemoglobin.

The conclusion that the cytosol hemoglobin is in contact, or nearly so, with the membrane, is in contrast to the observation that 2-AS in the membrane of intact erythrocytes remained unquenched when hemoglobin (2 mM heme) was added. It is concluded that exterior hemoglobin can approach no closer than ~60 Å to the outer surface of the phospholipid bilayer, possibly because the sugar moieties attached to certain membrane proteins prevent proteins from approaching the membrane.

The difference in phospholipid distribution between the inner and outer leaflets provides an alternative explanation for this observation. Phosphotidylserine, which carries a net negative charge, is found exclusively in the inner leaflet of the bilayer. The binding of hemoglobin to ghosts at acidic pH has been studied by different approaches (Shaklai et al., 1977, Salhany et al., 1977) and it has been noted that only the inner bilayer provides significant binding sites for hemoglobin (Szundi et al., 1980).

The present experiments yield estimated distances from the cytosol boundary layer to various donors in the membrane, and confirm that the series of *n*-AS probes are indeed located at different depths within the bilayer. This justifies their use to obtain a fluidity gradient across the phospholipid bilayer. While the steady-state anisotropy, $\langle r \rangle$ was found to have a minimum near the center of the bilayer, the interpretation of this result in terms of membrane fluidity must be approached with caution until anisotropy decay data becomes available (cf. Results section 1).

The data of Table II show that the hemoglobin density in the cytosol boundary layer is increased by 50% when the pH is lowered from 7.4 to 6.1. Unlike the greater increase in $\langle \rho/x^3 \rangle$, which is attainable in osmotically shrunken cells, the pH dependence of $h_b$ may reflect a specific interaction between hemoglobin and the inner membrane face, and may have physiological significance (Eisinger et al., 1982). It is noteworthy that when *n*-AS-labeled ghosts are titrated with hemoglobin at pH 6.2, much greater donor quenching is observed, but only at very low ionic strengths (Shaklai et al., 1977; Eisinger and Flores, 1982). This suggests that lysis and the subsequent washings produce changes in the membrane structure that make our model inapplicable and that alter the membrane's affinity for hemoglobin. It is therefore necessary to use care when studying hemoglobin-membrane interactions in ghost systems.

While the present work demonstrates the usefulness of our simple geometrical model for interpreting the quenching of fluorescent membrane probes caused by energy transfer to hemoglobin in normal erythrocytes, it would be a mistake to apply this model uncritically. It is possible that under certain stresses, (e.g., echinocytogenesis or sickling) the usual bilayer structure of the membrane is disrupted and micellelike structures may appear. This would alter the relative spatial distribution of probes and hemoglobin, and could produce the unusually efficient RET, which has in fact been observed in certain pathological cells and in ghost-hemoglobin titrations.

## APPENDIX

In the transverse RET model outlined in Methods section 3, the acceptors are assumed to form a constant-density, semiinfinite continuum whose

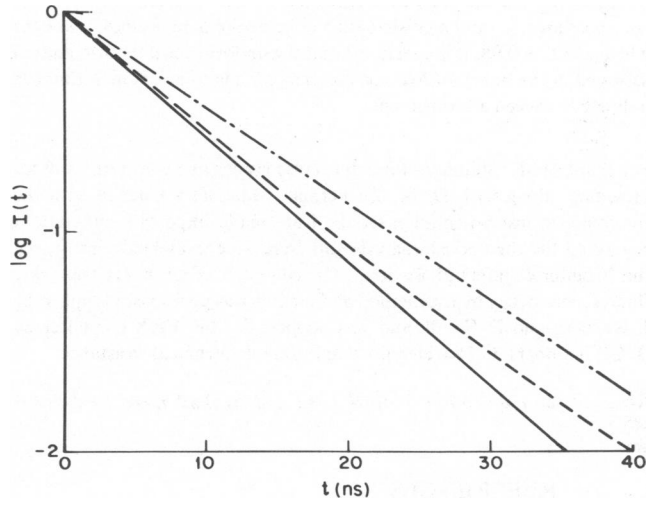


FIGURE 13 Impulse decay function of a donor ($\tau$ = 10 ns) in the absence of acceptors (- · · ·) and in the presence of the two-acceptor distributions discussed in the Appendix: the first uniform (—) and the other with maximum heterogeneity (- - -). The similarity of these simulated decays suggest that the lumpiness of the heme distribution in erythrocytes does not introduce significant errors in the RET efficiencies (cf. Eq. A3).

boundary plane is a distance $x(= d/R_0)$ from the donor plane. In a real erythrocyte, the acceptors (hemes) are grouped in tetramers and the hemoglobin molecules, assumed spherical with a diameter of 60 Å, have a packing fraction of ~0.3 so that the acceptor environment of individual donors can vary. This raises the question of whether the dynamic spatial averaging assumed in our model introduces a significant error into their semiempirical theory of Methods section 3.

To answer this question we investigated the effect on the donor fluorescence decay of two extreme acceptor distributions. In the first, all donors see the continuum of acceptors outlined above, and according to Eq. 11 their normalized impulse decay function is given by

$$I_1(t) = \exp(-k - k_T)t$$
$$= \exp\{-kt[1 + (\pi/6)(\rho/x^3)]\}. \quad \text{(A1)}$$

In the second acceptor distribution, a fraction $(1 - f)$ of the donors see no acceptors, while for a fraction $f$ the acceptor density is increased to $\rho/f$, so that the average acceptor density remains the same. The decay function is then

$$I_2(t) = (1 - f)\exp(-kt)$$
$$+ f\exp\{-kt[1 + (\pi/6)\rho/fx^3)]\}. \quad \text{(A2)}$$

The maximum packing that hemoglobin can achieve is only about twice that estimated for the boundary layer ($h_b \sim 15$ mM), so that $f = 0.5$ yields the most heterogeneous acceptor distribution we need to consider. Using parameters similar to those determined for 12-AS probes ($k \approx 0.1$ ns$^{-1}$, $\langle \rho/x^3 \rangle \approx 0.3$), the donor decay functions $I_1(t)$ and $I_2(t)$ were compared in Fig. 13, which also shows the impulse decay function of a donor in the absence of acceptors. It can be seen that the donor decays somewhat more slowly in the presence of a heterogeneous acceptor distribution.

The RET efficiencies corresponding to the decays $I_1(t)$ and $I_2(t)$ can be estimated by Eqs. 5 and 11, and their ratio is

$$\frac{T_2}{T_1} = \frac{1 + (\pi/6(\rho/x^3)}{1 + (\pi/6)(\rho/fx^3)}. \quad \text{(A3)}$$

For 12-AS probes this ratio has a value of 0.83 when $f = 0.5$, which shows that RET is 17% less efficient when the acceptor distributions seen by the donors is maximally heterogeneous. A more realistic estimate of $f$, coresponding to a random distribution of hemoglobin molecules, is 0.9, for which $T_2/T_1 \approx 0.98$. It is concluded that the uniform acceptor distribution assumed in the model of Methods section 3 leads to errors in $T$ that are unlikely to exceed a few percent.

We thank W. E. Blumberg for helpful discussions and comments and for providing, along with D. M. Zuckerman, valuable assistance with the fluorometric instrumentation. R. E. Dale made important suggestions regarding the theoretical analysis and Irene Kochevar kindly measured the (Coulter counter) ghost titres. The computer program for analyzing fluorescence decay by the method of moments was generously supplied by I. Isenberg and E. Small, and was adapted for the VAX computer by B. C. Chambers, F. Doleiden provided valuable technical assistance.

*Received for publication 7 April 1982 and in final form 14 October 1982.*

## REFERENCES

Badley, R. A., W. G. Martin, and H. Schneider. 1973. Dynamic behavior of fluorescent probes in lipid bilayer model membranes. *Biochemistry.* 12:268–275.

Bateman, J. B., S. S. Hsu, J. P. Knudsen, and K. L. Yudowitch. 1953. Hemoglobin spacing in erythrocytes. *Arch. Biochem. Biophys.* 45:411–422.

Branton, D., C. M. Cohen, and J. Tyler. 1981. Interaction of cytoskeletal proteins and the human erythrocyte membrane. *Cell.* 24:24–43.

Dale, R. E., I. A. Chen, and L. Brand. 1977. Rotational relaxation of the "microviscosity" probe diphenylhexatriene in paraffin oil and egg lecithin vesicles. *J. Biol. Chem.* 252:7500–7510.

Dale, R. E., J. Eisinger, and W. E. Blumberg. 1979. The orientational freedom of molecular probes. The orientation factor in intramolecular energy transfer. *Biophys. J.* 26:161–194.

Eisinger, J., and J. Flores. 1979. Front face fluorometery of liquid samples. *Anal. Biochem.* 94:15–21.

Eisinger, J., N. Boens, and J. Flores. 1981. Fluorescence polarization study of human erythrocyte membranes with 1-phenyl-3-(2-naphthyl)-2-pyrazoline as orientational probe. *Biochim. Biophys. Acta.* 646:334–343.

Eisinger, J., and Flores, J. 1982. The relative locations of intramembrane fluorescent probes and of the cytosol hemoglobin in erythrocytes, studied by transverse resonance energy transfer. *Biophys. J.* 37:6–7.

Eisinger, J., J. Flores, and J. M. Salhany. 1982. Association of cytosol hemoglobin with the membrane in intact erythrocytes. *Proc. Natl. Acad. Sci. USA.* 79:408–412.

Fairbanks, G., T. L. Steck, and D. F. H. Wallach. 1971. Electrophoretic analysis of the major polypeptides of the human erythrocyte membrane. *Biochemistry* 10:2606–2617.

Förster, Th. 1948. Zwischenmolekulare Energiewanderung und Fluoreszenz. *Ann. Physik.* 2:55–75.

Gratzer, W., and C. H. Beavin. 1979. Properties of the high molecular weight protein (spectrin) from human erythrocyte membranes. *Eur. J. Biochem.* 58:403–409.

Haigh, E. A., K. R. Thulborn, and W. H. Sawyer. 1979. Comparison of fluorescence energy transfer and quenching methods to establish the position and orientation of components within the transverse plane of a lipid bilayer. Application to the Gramicidin A-bilayer interaction. *Biochemistry.* 18:3525–3532.

Isenberg, I., and R. D. Dyson. 1969. The analysis of fluorescence decay by a method of moments. *Biophys. J.* 9:1337–1350.

Isenberg, I., R. D. Dyson, and R. Hanson. 1973. Studies on the analysis of fluorescence decay data by the method of moments. *Biophys. J.* 13:1090–1115.

Kawato, S. K., Kinosita, Jr., and A. Ikegami. 1977. Dynamic structure of lipid bilayers studied by nanosecond fluorescence techniques. *Biochemistry.* 16:2319–2324.

Lux, S. E. 1979. Dissecting the red cell membrane skeleton. *Nature* (Lond.) 281:426–429.

Matayoshi, E. D., and A. M. Kleinfeld. 1981. Emission wavelength-dependent decay of the 9-anthroyloxy-fatty acid membrane probes. *Biophys. J.* 35:215–235.

Mohandas, N., J. Wyatt, D. Shelton, and S. Shohet. 1980. Cross-linking of red cell cytoskeletal proteins increases transmembrane lipid movement. *Fed. Proc.* 39:1918.

Muirhead, H., J. M. Cox, L. Mazarella, and M. F. Perutz. 1967. Structure and function of haemoglobin. III. A three-dimensional Fourier synthesis of human deoxyhaemoglobin at 5.5Å resolution. *J. Mol. Biol.* 28:117–156.

Perutz, M. F. 1948. Submicroscopic structure of the red cell. *Nature (Lond.)* 161:204–205.

Salhany, J. M., K. A. Cordes, and E. D. Gains. 1977. Light-scattering measurements of hemoglobin binding to the erythrocyte membrane. Evidence for trans-membrane effects related to a disulfonic stilbene binding to band 3. *Biochemistry.* 19:447–1454.

Salhany, J. M., and K. C. Gaines. 1981. Connections between cytoplasmic proteins and the erythrocyte membrane. *Trends Biochem. Sci. January:* 13–15.

Shaklai, N., J. Yguerabide, and H. M. Ranney. 1977. Interaction of hemoglobin with red blood cell membranes as shown by a fluorescent chromophore. *Biochemistry.* 16:5585–5592.

Sheetz, M. P., and D. Sawyer. 1978. Triton shells of intact erythrocytes. *J. Supramol. Struct.* 8:399–412.

Shohet, S. B. 1981. Possible roles for the membrane cytoskeleton in regulating red cell stability and deformability. *Scand J. Clin. Lab. Invest. (Suppl.)* 41:123–130.

Shotton, D., B. Burk, and D. Branton. 1979. The molecular structure of human erythrocyte spectrin. *J. Mol. Biol.* 131:303–329.

Small, E. W., and I. Isenberg. 1977. On moment index displacement. *J. Chem. Phys.* 66:3347–3351.

Small, E. W., and I. Isenberg. 1983. Fluorescence decay analysis by the method of moments. Proceedings of the NATO Advanced Study Institute on Time-Resolved Fluorescence Spectroscopy in Biochemistry and Biology. In press.

Stamatoff, J. T., Bilash, Y. Ching and P. Eisenberger. 1979. X-ray scattering from labeled membranes. *Biophys. J.* 28:413–422.

Szundi, I., J. G. Szelenényi, J. H. Breuer, and A. Berczi. 1980. Interactions of hemoglobin with erythrocyte membrane phospholipids in monomolecular lipid layers. *Biochim. Biophys. Acta.* 595:41–46.

Thulborn, K. R., and W. H. Sawyer. 1978. Properties and locations of a set of fluorescent probes sensitive to the fluidity gradient of the lipid bilayer. *Biochim. Biophys. Acta.* 511:125–140.

Tilley, L., K. R. Thulborn, and W. H. Sawyer. 1979. An assessment of the fluidity gradient of the lipid bilayer as determined by a set of *n*-(9-anthroyloxy) fatty acids ($n$ = 2, 6, 9, 12, 16). *J. Biol. Chem.* 254:2592–2594.

Wilkins, M. H. F., A. E. Blaurock, and D. M. Engelman. 1971. Bilayer structure in membranes. *Nat. New Biol.* 230:72–76.

Waggoner, A. S., and L. Stryer. 1970. Fluorescent probes of biological membranes. *Proc. Natl. Acad. Sci. USA.* 67:579–589.

Wilson, J. E. 1978. *Trends Biochem. Sci.* 3:124–125.

Wolber, P. K., and B. S. Hudson. 1979. An analytical solution to the Förster energy transfer problem in two dimensions. *Biophys. J.* 28:197–210.